Title	Spatiotemporally quantitative in vivo imaging of mitochondrial fatty acid b-oxidation at cellular-level resolution in mice
Author(s)	Matsumoto, Ayumi; Matsui, Isao; Uchinomiya, Shohei et al.
Citation	American Journal of Physiology - Endocrinology and Metabolism. 2023, 325(5), p. E552-E561
Version Type	AM
URL	https://hdl.handle.net/11094/93228
rights	© 2023 the American Physiological Society.
Note	

1 Methods and Resources

3 Spatiotemporally quantitative *in vivo* imaging of
4 mitochondrial fatty acid β-oxidation at cellular-level
5 resolution in mice

6

7 Ayumi Matsumoto[1, 4], Isao Matsui*[, 1, 2, 4], Shohei Uchinomiya[3], Yusuke Katsuma[1], Seiichi

8 Yasuda[1], Hiroki Okushima[1], Atsuhiro Imai[1], Takeshi Yamamoto[1], Akio Ojida[3], Kazunori

9 Inoue[1], and Yoshitaka Isaka[1].

10

11 [1] Department of Nephrology, Osaka University Graduate School of Medicine, 2-2 Yamada-

12 oka, Suita, Osaka 565-0871, Japan

13 [2] Transdimensional Life Imaging Division, Institute for Open and Transdisciplinary

14 Research Initiatives, Osaka University, 2-1 Yamada-oka, Suita, Osaka 565-0871, Japan

15 [3] Department of Medical Chemistry and Chemical Biology, Graduate School of

16 Pharmaceutical Science, Kyushu University, 3-1-1 Maidashi, Higashi-Ku, Fukuoka 812-

17 8582, Japan

18 [4] These authors contributed equally

19

20 Correspondence: Isao Matsui (matsui@kid.med.osaka-u.ac.jp)

21 Department of Nephrology, Osaka University Graduate School of Medicine

22 2-2 Yamada-oka, Suita, Osaka 565-0871, Japan

23 Phone: +81-6-6879-3857; Fax: +81-6-6879-3230

ABSTRACT

Mitochondrial fatty acid β-oxidation (FAO) plays a key role in energy homeostasis. Several FAO evaluation methods are currently available, but they are not necessarily suitable for capturing the dynamics of FAO *in vivo* at a cellular-level spatial resolution and seconds-level time resolution. FAOBlue is a coumarin-based probe that undergoes β-oxidation to produce a fluorescent substrate, 7-hydroxycoumarin-3-(N-(2-hydroxyethyl))-carboxamide (7-HC). After confirming that 7-HC could be specifically detected using multiphoton microscopy at excitation/emission wavelength = 820/415-485 nm, wild-type C57BL/6 mice were randomly divided into control, pemafibrate, fasting (24 or 72 hours), and etomoxir groups. These mice received a single intravenous injection of FAOBlue. FAO activities in the liver of these mice were visualized using multiphoton microscopy at 4.2 seconds/frame. These approaches could visualize the difference in FAO activities between periportal and pericentral hepatocytes in the control, pemafibrate, and fasting groups. FAO velocity, which was expressed by the maximum slope of the fluorescence intensity curve, was accelerated in the pemafibrate and 72 hours fasting groups both in the periportal and the pericentral hepatocytes in comparison to the control group. Our approach revealed differences in the FAO activation mode by the two stimuli, *i.e.* pemafibrate and fasting, with pemafibrate accelerating the time of first detection of FAO-derived fluorescence. No increase in the fluorescence was observed in etomoxir-pretreated mice, confirming that FAOBlue specifically detected FAO *in vivo*. Thus, FAOBlue is useful for visualizing *in vivo* liver FAO dynamics at the single-cell level spatial resolution and seconds-level time resolution.

NEW & NOTEWORTHY

Fatty acid β-oxidation (FAO) plays a key role in energy homeostasis. Here, the authors established a strategy for visualizing FAO activity *in vivo* at the cellular-level spatial resolution and seconds-level time resolution in mice. Quantitative analysis revealed spatiotemporal heterogeneity in hepatic FAO dynamics. Our method is widely applicable because it is simple and uses a multiphoton microscope to observe the FAOBlue-injected mice.

INTRODUCTION

Mitochondrial fatty acid β-oxidation (FAO) is the primary metabolic pathway for the degradation of fatty acids and the maintenance of energy homeostasis.[1] Currently, there are several methods researchers use to analyze different aspects of FAO in various physiological and pathological conditions.[2–4] These include real-time PCR and immunoblots to analyze expression levels of critical FAO-related enzymes and regulators, real-time cell metabolic analysis to measure oxygen consumption rates, and mass spectrometry to analyze metabolic intermediate levels, and quantification of $^{3}H_2O$ or $^{14}CO_2$ converted from ^{3}H- or ^{14}C-labeled fatty acids.[5–10]

Subheading level 2

Understanding FAO dynamics *in vivo* is essential because inter-organ communication is critical in regulating FAO.[11, 12] However, the methods currently available are not necessarily suitable for capturing the spatiotemporal dynamics of FAO *in vivo* at the cellular-level spatial resolution and seconds-level time resolution.[13] Therefore, improvements in the FAO analysis method at these points can further enhance our understanding of FAO in pathophysiology.

Subheading level 3

Recently, we developed FAOBlue, a coumarin-based probe that can detect FAO activity in cultured cells.[14] FAOBlue is the compound described as probe **10** in our previous report, and it undergoes mitochondrial β-oxidation to produce 7-hydroxycoumarin-3-(N-(2-hydroxyethyl))-carboxamide (7-HC), a fluorescent substance described as coumarin **16** in our previous report.[14] Although we have reported that FAOBlue helps measure FAO activity *in vitro*, it was unknown whether the reagent was also helpful in measuring FAO in live animals. In this study, we established a method to evaluate the spatiotemporal dynamics of FAO *in vivo* at the cellular-level spatial resolution and seconds-level time resolution. Our method enables the visualization of FAO activity with simplicity and unprecedented spatiotemporal resolution.

MATERIALS AND METHODS

Mice studies

All animal experiments were approved by the Animal Committee of Osaka University,

90   Japan (approval number:02-006-006), and the study was performed in accordance with

91   the standard guidelines regarding the use of animals in scientific experiments. Six-week-

92   old male C57BL/6J mice were purchased from Japan SLC (RRID: IMSR_JAX:000664,

93   Hamamatsu, Japan) and were housed in groups of 2–3 at 22–24°C in a humidity-

94   controlled specific-pathogen-free room with a 12-hour light-dark cycle. Except for the

95   fasting specimens, all mice had *ad libitum* access to a regular chow diet (MFG diet;

96   Oriental Yeast, Tokyo, Japan).

97

98   **Compounds preparation**

99   FAOBlue (FDV-0033, Funakoshi, Tokyo, Japan) was dissolved in sterile-filtered

100   dimethyl sulfoxide (DMSO, 13408-64, Nacalai Tesque Inc., Kyoto, Japan) to prepare a 10

101   mM stock solution aliquoted in light-proof tubes and stored at −20°C until use. At the time

102   of use, FAOBlue was further diluted in a dilution buffer (normal saline containing 0.01%

103   Tween-20 and 0.2% ethanol). Pemafibrate (TQ0107, TargetMol, Boston, MA, USA) was

104   dissolved in DMSO at a concentration of 10 mg/ml to prepare a stock solution. Etomoxir

105   (E1905, Sigma-Aldrich, St Louis, MO, USA) was dissolved in normal saline at the time of

106   use. 7-HC was synthesized as previously described by Uchinomiya *et al*. and dissolved in

107   DMSO to prepare a 10 mM stock solution.(14)

108

109   **Experimental treatment and imaging preparations**

110   To analyze hepatic lobule structure, Texas Red™ conjugated 70 kDa dextran (D1830,

111   Invitrogen, Waltham, MA, USA) dissolved in normal saline at 500 µg/ml was intravenously

112   injected (100 µl/animal) through the right jugular vein. The FAO activity was visualized

113   with a single intravenous injection of diluted FAOBlue (62.5 µM, 100 µl/animal) through the

114   right jugular vein. To evaluate FAO activity, the mice were randomly divided into five

115   groups: control (Ctrl), pemafibrate (Pema), fasting for 24 hours (Fasting_24h), fasting for 72

116   hours (Fasting_72h), and etomoxir (Eto). The FAO activity in the Ctrl group was evaluated

117   without any specific pretreatment. Mice in the Pema group were administered pemafibrate

118   (0.1 mg/kg body weight (BW)) suspended in methylcellulose 400 (133–17815, FUJIFILM

119   Wako Pure Chemicals, Osaka, Japan) by oral gavage at 24 and 1 h before imaging. Mice

120   in the Fasting_24h and Fasting_72h groups were fasted for 24 h and 72 h prior to imaging,

121   respectively. Mice in the Eto group were intraperitoneally administered etomoxir (20 mg/kg

122   BW) dissolved in normal saline at 12 h and 1 h before the imaging. All the animal

123   experiments were performed in the morning. For *in vivo* imaging, the mice were

124   anesthetized with an intraperitoneal injection of medetomidine, midazolam, and

125   butorphanol. A 30-gauge catheter was inserted into the right jugular vein for reagent

126   injection. The left lobe of the liver was exteriorized through a small flank incision and was

127   placed on a cover glass. The microscope stage had a heater to keep the body temperature

128   at 36–38°C. Another heater maintained the temperature inside the microscope cover at

129   36–38°C. When studying the kinetics of exogenously administered 7-HC, rather than 7-HC

130   resulting from FAOBlue metabolism, 7-HC (2.5 μM, 100 μl/animal) was intravenously

131   injected through the right internal jugular vein. The observations of the 7-HC-injected mice

132   were conducted in the same way as in the FAOBlue-injected mice. No animals reached

133   humane endpoints, and no unexpected adverse events occurred during the experiments.

134

135   **Multiphoton microscopy**

136   All *in vivo* images were obtained using a Nikon A1R MP+ multiphoton microscope

137   (Nikon, Tokyo, Japan) equipped with a 20× water-immersion objective lens. Excitation was

138   performed using the Chameleon Discovery laser system (Coherent Inc., Santa Clara, CA,

139   USA). A combination of 820 nm excitation and a 450/70 bandpass filter was used to detect

140   the 7-HC signals. To visualize dextran conjugated with Texas Red[TM] dye, a combination of

141   1080 nm excitation and a 593/46 bandpass emission filter was used. Images were

142   obtained continuously before and after the dye injection. For the FAOBlue analyses, the

143   laser power, photomultiplier tube high voltage (PMT HV), and PMT offsets were set to

144   6.5%, 130 V, and 0 V, respectively. These parameters were set to 7.5 %, 100 V, and 0 V,

145   respectively, for Texas Red[TM] dye-conjugated dextran. Animals for which data could not be

146   obtained due to body movements during microscopic observation were excluded from the

147   analysis.

148

149   **Experiments to confirm the fluorescent properties of FAOBlue and 7-HC**

150   To confirm that 7-HC, but not FAOBlue, was fluorescent under our experimental

151   conditions, 7-HC and FAOBlue solutions were dropped on the coverslip and directly

152   observed using a Nikon A1R MP+ multiphoton microscope under the same

153   excitation/emission conditions as *in vivo* imaging for FAO. The samples were diluted using

154   the dilution buffer used in the animal experiments. The fluorescence spectra of FAOBlue

155   and 7-HC were measured in a similar manner by changing the excitation wavelength in 10

156   nm increments in the range of 710-1020 nm.

157

158   **Video**

159   The video was prepared using Numpy 1.19.5, a Python library for scientific computing,

160   and Imageio 2.26.0, a Python library that provides an interface for reading and writing a

161   wide range of images. Acquisition of multiphoton microscopy images took 4.2 sec/frame.

162   Videos of FAOBlue- or 7-HC-injected mice were recorded at 10 frames/s, while Texas

163   Red[TM] dextran-injected mice were recorded at 5 frames/s. Thus, the FAOBlue- or 7-HC-

164 related video has a rate of 42 ×, whereas the Texas Red^{TM} dextran-related video has a

165 rate of 21 ×.

166

167 **Real-time PCR**

168   Real-time SYBR Green PCR was performed to quantify mRNA expression using a

169 QuantStudio 7 Flex system (Applied Biosystems, Waltham, MA, USA). The primer sets are

170 shown in Supplemental Table S1. RNA was extracted using TRIzol reagent (Invitrogen)

171 according to the manufacturer's instructions.

172

173 **Histological analyses**

174   The liver tissues were fixed in 4.0% paraformaldehyde in phosphate-buffered saline.

175 Hematoxylin and eosin (HE) staining of paraffin-embedded sections was carried out using the

176 standard methods. All images of HE-stained sections were obtained using an Eclipse Ni

177 microscope (Nikon, Tokyo, Japan).(15)

178

179 **Quantification of the multiphoton microscopic images**

180   To quantitatively evaluate the fluorescence intensity, small circular regions of interest

181 (ROIs) with a radius of 4 pixels were placed in the cytoplasmic regions of the images.

182 Since FAO does not occur in the nucleus and FAOBlue metabolite (*i.e.*, 7-HC) is excreted

183 into the bile canaliculi, a 4-pixel ROI was set up to measure fluorescence only in the

184 cytoplasmic region, not overlapping the nuclei and canaliculi regions. At least ten ROIs per

185 animal were measured in the periportal and pericentral regions. ROIs were not selected

186   with multiple ROIs/cell but one ROI/cell. Because the baseline autofluorescence intensity

187   varied according to the location within the hepatic lobule and by pretreatments, the

188   fluorescence levels were calculated using the mean intensity of the first three frames as 0.

189   Nikon A1R MP+ multiphoton microscopy returned a 12-bit (*i.e.*, 0-4095 grayscale) image,

190   which was converted to an 8-bit (*i.e.*, 0-255 grayscale) image for quantification.(16) The

191   area under the curve (AUC) was calculated by adding the average fluorescence intensity of

192   each region in each frame per animal. The maximum slope was defined as the maximum

193   of the increasing slopes calculated for every five frames of the intensity curve for each

194   animal. The time of the first detection of FAO-derived fluorescence was defined as the

195   point in each ROI when the FAO-derived fluorescence exceeded three standard deviation

196   (SD) values of the first five frames. The time to the fluorescence peak was defined as the

197   average time from the start of observation until reaching the top three points of

198   fluorescence intensity. The rate of decay from the fluorescence peak was calculated by

199   dividing the difference in the fluorescence intensity between at the peak and 7 min by the

200   time between the fluorescent peak and 7 min.

201

202   **Statistical analyses**

203   A *t*-test was used to evaluate significant differences between two groups. Multiple group

204   comparisons were performed using the Dunnett's test. Statistical significance was defined

205   as *P* < 0.05. All data were analyzed using JMP software (SAS Institute, Cary, NC, USA).

206   All results are presented as means ± SD. The number of replicates is mentioned in the

207   figure legends.

208

RESULTS

Set up for FAOBlue multiphoton microscopy

To visualize the spatiotemporal dynamics of FAO *in vivo*, we analyzed FAOBlue-injected mice using multiphoton microscopy. Before administering FAOBlue to mice, we tested whether 7-HC could be specifically detected under our microscopic conditions since we have reported that FAOBlue and 7-HC have absorption peaks at 350 and 405 nm in single-photon excitation, respectively.(14) We analyzed the fluorescence spectrum using different two-photon excitation wavelengths (λ_{ex}) and a 415-485 nm emission filter (λ_{em}) (Figure 1A). Under the conditions used in the following animal experiments ($\lambda_{ex}/\lambda_{em}$ = 820/415-485 nm), FAOBlue was not fluorescent, whereas 7-HC increased its fluorescence intensity in a concentration-dependent manner (Figures 1A, B, and Supplemental Figure S1A). We also performed HE-staining of the liver to test whether FAOBlue is toxic. The results showed no obvious difference between the liver of vehicle- and FAOBlue-treated mice (Supplemental Figure S1B).

Identification of hepatic lobular structures under the 820/415-485 nm condition

Constituent cells of the liver form functional segments, namely periportal and pericentral hepatocytes, in the hepatic lobules. Thus, we tested whether FAOBlue can be used to visualize differences in FAO activity for each functional segment rather than the whole organ. Mouse settings for multiphoton microscope analyses are shown in Supplemental Figure S2. Step-by-step instructions and troubleshooting tips are summarized in Supplemental Information. The normal liver showed strong autofluorescence in hepatic stellate cells (bright dots in Figure 1C(a) and (b)).

233 Hepatocytes were also visualized using autofluorescence, and the autofluorescence level

234 was relatively strong in the areas indicated by the dashed white lines in Figure 1C(a). To

235 make it easier to observe the difference in the autofluorescence levels between the area

236 enclosed by the dashed line and the rest, a figure in which the grayscale has been

237 adjusted is shown in Figure 1C(c). It has been reported that autofluorescence of

238 hepatocytes helps identify the anatomy of the lobule. To determine this anatomy under the

239 $\lambda_{ex}/\lambda_{em}$ = 820/415-485 nm condition, we analyzed which part of the hepatic lobule the area

240 enclosed by the white dashed line corresponds to. Analysis of Texas Red^{TM} dextran (70

241 kDa)-injected mice revealed that blood flowed toward the area surrounded by the white

242 dashed line (Figure 1C(d)-(g), and Supplemental Video S1). Therefore, the enclosed areas

243 are the pericentral regions of the hepatic lobules.

244

245 **Spatiotemporal quantification of FAO activity in the liver revealed a difference**

246 **in FAO activation mode between pemafibrate and fasting**

247   To visualize FAO activity in the liver, six- to seven-week-old male C57BL/6J mice were

248 randomly divided into five groups: Ctrl, Pema, Fasting_24h, Fasting_72h, and Eto (Figure

249 2). Mice in the Ctrl group received no pretreatment. Mice in the Pema and Eto groups

250 were pretreated with pemafibrate, a selective peroxisome proliferator-activated receptor α

251 (PPARα) modulator, and etomoxir, an inhibitor of mitochondrial carnitine palmitoyl

252 transferase 1 (CPT1), respectively. Mice in the Fasting_24h and Fasting_72h groups were

253 fasted for 24 or 72 hours, respectively. Since PPARα is a key regulator of gene expression

254 involved in FAO, and fasting triggers fat mobilization from adipose tissues, we anticipated

255 FAO activation in both the Pema and the two fasting groups.(17, 18) Conversely, as CPT1

256 is the rate-limiting enzyme for FAO, we expected FAO to be suppressed in the Eto

257 group.(19) The FAO activity was visualized with a single intravenous injection of FAOBlue.

258 Representative liver images of the Ctrl and pretreated mice are shown in Figure 2 and

259 Supplemental Video S2.

260 We quantified fluorescent intensities of hepatocytes by setting circular ROIs with a

261 radius of 4 pixels (Figure 3 and Supplemental Figure S3A). It was previously reported that

262 FAOBlue-treated HepG2 cells gradually increased FAO-derived fluorescence in a time-

263 dependent manner up to 30 min, however, the fluorescent signal of the periportal region in

264 the Ctrl, Pema, Fasting_24h, and Fasting_72h groups peaked much earlier (Figures 2, 3A

265 and Supplemental Video S2).(14) Because CPT1 activity in HepG2 cells has been shown

266 to be lower than that in parenchymal hepatocytes, low CPT1 activity in HepG2 cells may

267 explain the reason why FAO-derived fluorescence in HepG2 cells increased slower than *in*

268 *vivo.*(20) Strong fluorescence signals were detected in the bile canaliculi at about the

269 same time that FAO activity was observed in the hepatocytes, suggesting that the 7-HC

270 was actively excreted into the canaliculi (Supplemental Figure S3B). No increase in

271 fluorescence was observed in the Eto group, confirming that FAOBlue specifically

272 detected mitochondrial FAO *in vivo*. The AUCs in Figure 3A for the Pema, Fasting_24h,

273 and Fasting_72h groups were higher than those of the Ctrl group in both the periportal and

274 pericentral regions, though the elevation in the pericentral region of the Fasting_24h group

275 was marginal (Figure 3B). The periportal AUCs were higher than the pericentral AUCs in

276 all groups, except for the Eto group (Figure 3A and Supplemental Figure S3C). We also

277 measured the increasing slope of the intensity curve every five frames and determined the

278 maximum intensity slope for each animal. The Pema and Fasting_72h groups, but not

279 Fasting_24h group, showed increased maximum slopes of the intensity curve compared

280 with the Ctrl group in both hepatic lobular regions (Figure 3C). The maximum intensity

281 slope of the periportal region was higher than that of the pericentral region in all groups

282   except for the Eto group (Supplemental Figure S3D). The differences in AUC and

283   maximum slope between the Ctrl and Eto groups were significant in the periportal region

284   but not in the pericentral region, showing that FAO in the Ctrl group occurred mainly in the

285   periportal region, with few FAO in the pericentral region (Figures 3B and 3C). Although the

286   pemafibrate and fasting treatments both stimulate FAO, FAOBlue-based spatiotemporal

287   analyses revealed that these interventions activate FAO differently. The first detection of

288   FAO-derived fluorescence in the Pema group was significantly earlier than that in the Ctrl,

289   but not different between the Fasting_24h or Fasting_72h group and the Ctrl groups

290   (Figures 3A and 3D). Real-time PCR analyses of FAO-related genes in the liver showed

291   that the levels of *Cpt1a* were elevated in the Pema, Fasting_24h and Fasting_72h groups

292   compared to that in the Ctrl group (Figure 3E). *Cpt1* mRNA expression was also elevated

293   in the Eto group, which seems be a compensatory response to FAO suppression. The

294   mRNA level of *Ppara*, encoding PPARα, the key regulator of FAO, was elevated in the

295   FAO-stimulated groups, *i.e.*, the Pema, Fasting_24h, and Fasting_72h groups, but the

296   downstream gene expression levels were not uniform among the groups. *Cpt2* mRNA

297   expression was elevated in the Pema and Fasting_24h groups but not in the Fasting_72h

298   group. The expression levels of *Ppargc1a*, encoding peroxisome proliferator-activated

299   receptor gamma coactivator 1-alpha (PGC1a), a master regulator of mitochondrial

300   biogenesis, were elevated in the Fasting_24h group but not in the Pema and Fasting_72h

301   groups. The levels of *Cd36*, a molecule that facilitates fatty acid uptake, were induced by

302   pemafibrate, but not by fasting. Therefore, the earlier FAO detection time in the Pema

303   group may be due to enhanced fatty acid uptake by hepatocytes.

304   The results shown in Figures 1-3 indicated that FAOBlue is useful for visualizing FAO

305   activation by various stimulations, as well as for illustrating the differences in FAO

306   activities between the periportal and pericentral regions of the liver. However, to make an

307 accurate assessment, there were several additional aspects that needed to be clarified.

308 For example, if the speed at which 7-HC is excreted to the bile canaliculi varies among the

309 experimental groups, group comparisons might not be conducted appropriately.

310 Furthermore, 7-HC, resulting from FAO in other organs and circulating in the blood

311 vessels, might be taken up primarily in the periportal region, leading to the results shown

312 in Figures 2 and 3. To address these issues, we analyzed the kinetics of 7-HC by

313 administrating 7-HC through the right jugular vein. In this experiment, the 7-HC dosage

314 was set at 0.25 nmol/animal (2.5 µM solution, 100 µl/animal), a reduction from the

315 FAOBlue amount of 6.25 nmol/animal (62.5 µM solution, 100 µl/animal) used in the

316 experiments shown in Figures 2 and 3. The purpose of this reduction was to determine

317 whether the amount of 7-HC administered into the vasculature, even at a dosage that

318 would result in fluorescent intensity comparable to that in the periportal region of the Ctrl

319 group treated with FAOBlue, would be sufficient to reach the pericentral region. As a

320 result, the fluorescence intensity increased in both the periportal and pericentral regions

321 immediately after the 7-HC administration (Figures 4, 5, and Supplemental Video S3). The

322 AUC of the fluorescence curve, the time to peak fluorescence, and the rate of decay from

323 the fluorescence peak were similar, irrespective of pretreatment or whether in the

324 periportal or pericentral region (Figures 4, 5, Supplemental Figure S4, and Supplemental

325 Video 3). Therefore, the comparisons of FAO among groups and between pericentral and

326 periportal regions can be conducted appropriately using FAOBlue.

327

DISCUSSION

329   This study demonstrated that FAOBlue is a useful tool for the spatiotemporal

330 quantification of FAO in mice liver. Our method shows that (1) FAO occurs mainly in the

331   periporal region; (2) the two FAO-activating stimuli, pemafibrate and fasting for 72 hours,

332   activate FAO in both the periportal and pericentral regions in terms of FAO quantity and

333   velocity, which are expressed by the AUCs and maximum increasing slope of the

334   FAOBlue-derived fluorescence intensity curve, respectively; (3) The Fasting_24h and

335   Fastign_72h groups increas the FAO quantity compared to the Ctrl group, with the

336   pericentral region of the Fasting_24h group showing marginal significance. The FAO

337   velocity increases in the Fasting_72h group, but not in the Fasting_24h group, indicating

338   that the pattern of FAO varies with the duration of fasting; and (4) both pemafibrate and

339   fasting are FAO-activating stimuli, but the time of first detection of FAO-derived

340   fluorescence is different. Our method is widely applicable because it is simple and uses a

341   multiphoton microscope to observe the FAOBlue-injected mice.

342   Spatial heterogeneity of hepatocytes has been reported since the early 20th century.

343   Kater *et al*. showed gradients along the porto-central axis in deposition levels of glycogen

344   and fat, as well as mitochondrial morphology in 1933.(21) Deane demonstrated that

345   periportal hepatocytes have larger mitochondria and less deposition of fat and coined the

346   term 'zonation' in 1944.(22) Following these pioneering morphology-based studies,

347   Braeuning *et al*. analyzed the overall picture of mRNA expression levels in the hepatic

348   zone using microarray. They isolated periportal and pericentral hepatocytes using the

349   digitonin-collagenase perfusion technique and showed that periportal hepatocytes express

350   higher levels of FAO-related genes than pericentral hepatocytes.(23) More recently,

351   Halpern *et al.* performed single-cell RNA sequencing of the mouse liver and revealed the

352   zonation profiles of liver gene expressions with high spatial resolution.(24) Although these

353   studies have led to considerable advances in liver research, the mere expression of FAO-

354   related enzymes does not necessarily translate into FAO activation. The hepatic zonation

355   was dynamic rather than static. For example, Guzmán *et al*. showed that oxidation of [14]C-

356 labeled palmitate was very flexible and changed markedly with the animal's physiological

357 status.(25) Therefore, evaluating the FAO activity directly is essential. Our method is

358 superior to previous methods in terms of radioisotope-free and high spatiotemporal

359 resolution.

360   FAOBlue has a structure consisting of a fatty acid with a carbon chain length of nine (C9) and

361 7-HC. In contrast to long-chain fatty acids, whose conversion to long-chain acyl-carnitine

362 species via CPT1 is required for mitochondrial transport, short- and medium-chain fatty

363 acids can enter mitochondria in a carnitine-independent manner. However, CPT1 was

364 required for the β-oxidation of FAOBlue, whose carbon chain length belongs to the medium

365 chain. This is not simply because C9 bound to 7-HC resulted in a longer structure; we have

366 previously shown that C5 (short-chain) bound 7-HC probe scarcely underwent β-oxidation

367 even in the absence of etomoxir.(14) We have also demonstrated that C9 probe that possesses

368 rhodol or naphthalimide as a fluorophore did not undergo any structural change upon incubation

369 with the HepG2 cells.(14) Therefore, the combination of C9 and 7-HC was optimal for CPT-1-

370 dependent mitochondrial transport, though the structural basis remains uncertain. Acyl-CoA

371 dehydrogenases (ACADs) are enzymes that catalyze the initial double-bound introduction step

372 of mitochondrial FAO. Based on substrate preference, ACADs are classified into several types:

373 short-, medium-, long-, and very long-chain ACADs. They are most active with 4C-, 8C-, 14C-,

374 and 16C-substrates, respectively.(26) Because substrates whose acyl chain length is too long

375 for a particular ACAD are excluded, while short-chain substrates bind weakly to ACADs specific

376 for longer substrates, the initial introduction of double-bound to FAOBlue is likely mediated by

377 medium- or longer-chain ACADs.(26) In the later cycles of FAO, short-chain ACAD might also

378 be responsible for the double-bound introduction.

379   The results shown in Figures 4, 5, and Supplemental Figure S4 showed that there are

380 no differences in the excretion of 7-HC from hepatocytes to the bile canaliculi, either

381   among the experimental groups or between the periportal and pericentral regions. This

382   finding corroborates the validity of the group and the region comparisons depicted in

383   Figure 3B-D and Supplemental Figure S3C-D. However, the fluorescence observed in

384   Figure 3A, following the peak period of fluorescence intensity, is likely to represent the

385   fluorescence of 7-HC produced by FAO at earlier phases and not yet excreted, rather than

386   the fluorescence of 7-HC generated by FAO of FAOBlue at that particular time point.

387   This study has several limitations. First, FAOBlue is unsuitable for observing deep in

388   organs because the fluorescence wavelength of 7-HC is short. Second, although our data

389   suggested that 7-HC generated in the liver was excreted mainly through the canaliculi,

390   details of how 7-HC generated in other organs is distributed or excreted are still unclear.

391   These issues should be addressed in future studies.

392   In conclusion, we demonstrated that observing FAOBlue-injected mice by multiphoton

393   microscopy is helpful for analyzing the spatiotemporal dynamics of FAO. It also helps

394   explore new insights into FAO.

395

DATA AVAILABILITY

396

Lead Contact

397

398   • Further information and requests for resources and reagents should be directed to

399   and will be fulfilled by the Lead Contact, Isao Matsui (matsui@kid.med.osaka-

400   u.ac.jp).

401

Materials availability

402

403   • This study did not generate any unique materials.

404

Data and Code Availability

- The image quantification code is available at
  https://github.com/NephrologyOsakaUniv/2023_FAOBlue/blob/main/2023_FAO_qua
  ntification.ipynb

409

SUPPLEMENTAL MATERIAL

Supplemental Information and legends, Supplemental Videos S1, S2 and S3:

https://figshare.com/s/df059d995711463d359a

413

ACKNOWLEDGMENTS

420

GRANTS

424

DISCLOSURES

The authors declare no competing interest.

AUTHOR CONTRIBUTIONS

AM, IM, SU, YK conceived and designed research; AM, YK, SY, HO, AI, TY performed experiments, analyzed data, interpreted results of experiments; AM, IM prepared figures, AM, IM drafted manuscript; IM, SU, AO, KI edited and revised manuscript; IM, AO, YI approved final version of manuscript.

REFERENCES

1. **Houten SM**, **Violante S**, **Ventura F V.**, **Wanders RJA**. The Biochemistry and Physiology of Mitochondrial Fatty Acid β-Oxidation and Its Genetic Disorders. *Annu Rev Physiol* 78: 23–44, 2016. doi: 10.1146/ANNUREV-PHYSIOL-021115-105045.

2. **Li Z**, **Zhang H**. Reprogramming of glucose, fatty acid and amino acid metabolism for cancer progression. *Cellular and Molecular Life Sciences 2015 73:2* 73: 377–392, 2015. doi: 10.1007/S00018-015-2070-4.

3. **Zhang L**, **Keung W**, **Samokhvalov V**, **Wang W**, **Lopaschuk GD**. Role of fatty acid uptake and fatty acid beta-oxidation in mediating insulin resistance in heart and skeletal muscle. *Biochim Biophys Acta* 1801: 1–22, 2010. doi: 10.1016/J.BBALIP.2009.09.014.

4. **Kang HM**, **Ahn SH**, **Choi P**, **Ko YA**, **Han SH**, **Chinga F**, **Park ASD**, **Tao J**, **Sharma K**, **Pullman J**, **Bottinger EP**, **Goldberg IJ**, **Susztak K**. Defective fatty acid oxidation in renal tubular epithelial cells has a key role in kidney fibrosis development. *Nature Medicine 2014 21:1* 21: 37–46, 2014. doi: 10.1038/nm.3762.

5. **Yamamoto T**, **Takabatake Y**, **Minami S**, **Sakai S**, **Fujimura R**, **Takahashi A**, **Namba-Hamano T**, **Matsuda J**, **Kimura T**, **Matsui I**, **Kaimori JY**, **Takeda H**, **Takahashi M**, **Izumi Y**, **Bamba T**, **Matsusaka T**, **Niimura F**, **Yanagita M**, **Isaka Y**. Eicosapentaenoic acid attenuates renal lipotoxicity by restoring autophagic flux. *Autophagy* 17: 1700–1713, 2021. doi: 10.1080/15548627.2020.1782034.

453 6.   **Mori D**, **Matsui I**, **Shimomura A**, **Hashimoto N**, **Matsumoto A**, **Shimada K**, **Yamaguchi S**, **Oka T**,
454   **Kubota K**, **Yonemoto S**, **Sakaguchi Y**, **Takahashi A**, **Shintani Y**, **Takashima S**, **Takabatake Y**,
455   **Hamano T**, **Isaka Y**. Protein carbamylation exacerbates vascular calcification. *Kidney Int* 94, 2018.
456   doi: 10.1016/j.kint.2018.01.033.

457 7.   **Chace DH**, **Kalas TA**, **Naylor EW**. Use of tandem mass spectrometry for multianalyte screening of
458   dried blood specimens from newborns. *Clin Chem* 49: 1797–1817, 2003. doi:
459   10.1373/CLINCHEM.2003.022178.

460 8.   **Nomura M**, **Liu J**, **Rovira II**, **Gonzalez-Hurtado E**, **Lee J**, **Wolfgang MJ**, **Finkel T**. Fatty acid
461   oxidation in macrophage polarization. *Nature Immunology 2016 17:3* 17: 216–217, 2016. doi:
462   10.1038/ni.3366.

463 9.   **Manning NJ**, **Olpin SE**, **Pollitt RJ**, **Webley J**. A comparison of [9,10-3H]palmitic and [9,10-
464   3H]myristic acids for the detection of defects of fatty acid oxidation in intact cultured fibroblasts.
465   *J Inherit Metab Dis* 13: 58–68, 1990. doi: 10.1007/BF01799333.

466 10. **Guzman M**, **Bijleveld C**, **Geelen MJH**. Flexibility of zonation of fatty acid oxidation in rat liver.
467   *Biochem J* 311: 853–860, 1995. doi: 10.1042/BJ3110853.

468 11. **Ito M**, **Adachi-Akahane S**. Inter-organ communication in the regulation of lipid metabolism:
469   focusing on the network between the liver, intestine, and heart. *J Pharmacol Sci* 123: 312–317,
470   2013. doi: 10.1254/JPHS.13R09CP.

471 12. **Whitehead A**, **Krause FN**, **Moran A**, **MacCannell ADV**, **Scragg JL**, **McNally BD**, **Boateng E**, **Murfitt
472   SA**, **Virtue S**, **Wright J**, **Garnham J**, **Davies GR**, **Dodgson J**, **Schneider JE**, **Murray AJ**, **Church C**,
473   **Vidal-Puig A**, **Witte KK**, **Griffin JL**, **Roberts LD**. Brown and beige adipose tissue regulate systemic
474   metabolism through a metabolite interorgan signaling axis. *Nature Communications 2021 12:1*
475   12: 1–21, 2021. doi: 10.1038/s41467-021-22272-3.

476 13. **Cunningham RP**, **Porat-Shliom N**. Liver Zonation - Revisiting Old Questions With New
477   Technologies. *Front Physiol* 12, 2021. doi: 10.3389/FPHYS.2021.732929.

478 14. **Uchinomiya S**, **Matsunaga N**, **Kamoda K**, **Kawagoe R**, **Tsuruta A**, **Ohdo S**, **Ojida A**. Fluorescence
479   detection of metabolic activity of the fatty acid beta oxidation pathway in living cells. *Chem
480   Commun (Camb)* 56: 3023–3026, 2020. doi: 10.1039/C9CC09993J.

481 15. **Matsui I**, **Hamano T**, **Mikami S**, **Inoue K**, **Shimomura A**, **Nagasawa Y**, **Michigami T**, **Ohnishi T**,
482   **Fujii N**, **Nakano C**, **Kusunoki Y**, **Kitamura H**, **Iwatani H**, **Takabatake Y**, **Kaimori J**, **Matsuba G**,
483   **Okoshi K**, **Kimura-Suda H**, **Tsubakihara Y**, **Rakugi H**, **Isaka Y**. Retention of fetuin-A in renal
484   tubular lumen protects the kidney from nephrocalcinosis in rats. *American Journal of Physiology-
485   Renal Physiology* 304: F751–F760, 2013. doi: 10.1152/ajprenal.00329.2012.

486 16. **Matsumoto A**, **Matsui I**, **Katsuma Y**, **Yasuda S**, **Shimada K**, **Namba-Hamano T**, **Sakaguchi Y**,
487   **Kaimori J**, **Takabatake Y**, **Inoue K**, **Isaka Y**. Quantitative Analyses of Foot Processes,
488   Mitochondria, and Basement Membranes by Structured Illumination. *Kidney Int Rep* 6: 1923–
489   1938, 2021. doi: 10.1016/j.ekir.2021.04.021.

490 17. **Pawlak M**, **Lefebvre P**, **Staels B**. Molecular mechanism of PPARα action and its impact on lipid
491 metabolism, inflammation and fibrosis in non-alcoholic fatty liver disease. *J Hepatol* 62: 720–33,
492 2015. doi: 10.1016/j.jhep.2014.10.039.

493 18. **Rakhshandehroo M**, **Knoch B**, **Müller M**, **Kersten S**. Peroxisome proliferator-activated receptor
494 alpha target genes. *PPAR Res* 2010, 2010. doi: 10.1155/2010/612089.

495 19. **Schlaepfer IR**, **Joshi M**. CPT1A-mediated Fat Oxidation, Mechanisms, and Therapeutic Potential.
496 *Endocrinology* 161, 2020. doi: 10.1210/endocr/bqz046.

497 20. **Agius L**. Metabolic interactions of parenchymal hepatocytes and dividing epithelial cells in co-
498 culture. *Biochem J* 252, 1988. doi: 10.1042/bj2520023.

499 21. **Kater JM**. Comparative and experimental studies on the cytology of the liver. *Für Zellforsch*
500 *Mikrosk Anat* 17: 217–246, 1933.

501 22. **Deane HW**. A cytological study of the diurnal cycle of the liver of the mouse in relation to storage
502 and secretion. *Anat Rec* 88: 39–65, 1944.

503 23. **Braeuning A**, **Ittrich C**, **Köhle C**, **Hailfinger S**, **Bonin M**, **Buchmann A**, **Schwarz M**. Differential
504 gene expression in periportal and perivenous mouse hepatocytes. *FEBS Journal* 273: 5051–5061,
505 2006. doi: 10.1111/J.1742-4658.2006.05503.X.

506 24. **Halpern KB**, **Shenhav R**, **Matcovitch-Natan O**, **Tóth B**, **Lemze D**, **Golan M**, **Massasa EE**, **Baydatch**
507 **S**, **Landen S**, **Moor AE**, **Brandis A**, **Giladi A**, **Stokar-Avihail A**, **David E**, **Amit I**, **Itzkovitz S**. Single-
508 cell spatial reconstruction reveals global division of labor in the mammalian liver. *Nature* 542:
509 352, 2017. doi: 10.1038/NATURE21065.

510 25. **Guzman M**, **Bijleveld C**, **Geelen MJH**. Flexibility of zonation of fatty acid oxidation in rat liver.
511 *Biochem J* 311: 853–860, 1995. doi: 10.1042/BJ3110853.

512 26. **Mander L**, **Liu HW**. Comprehensive Natural Products II: Chemistry and Biology. 2010.

513

FIGURE LEGENDS

Figure 1. Multiphoton microscope set up

516 (A) Fluorescence spectra of FAOBlue and 7-Hydroxycoumarin-3-(N-(2-hydroxyethyl))-

517 carboxamide (7-HC) under the excitation of a two-photon laser. The fluorescence intensity of

518 FAOBlue (62.5 µM) or 7-HC (0.3125 µM) dissolved in a dilute buffer was measured using a two-

519 photon microscope (λ_{em} = 415-585 nm). The horizontal axis represents the excitation

520 wavelength of the two-photon microscope. The original microscopic images were 12-bit

grayscale but were converted to 8-bit grayscale (0–255 scale) for analysis. The vertical axis of the graph represents the average grayscale of the acquired images (*i.e.*, fluorescence intensity) (N = 5 in each measurement). (B) The signal intensities of the dilution buffer, FAOBlue, and 7-HC solution ($\lambda_{ex}/\lambda_{em}$ = 820/415-485 nm). The regression line for 7-HC was drawn using measurements within the concentration range of 0 to 0.625 µM (N = 5 in each measurement: R^2 = 0.9916). All results are presented as the means ± standard deviations (SDs). (C) (a)–(d) Representative liver images at baseline and (e)-(g) the first frame in which injected Texas Red™ dextran (70 kDa) appeared (Scale bars: 100 µm). See Supplemental Video S1. (a) and (c)-(g) are observations of the same region. The orange square in (a) was enlarged in (b). (a) White dashed circles indicate areas where hepatocytes have relatively strong autofluorescence. To make it easier to see the difference in hepatocyte autofluorescence in (a), the signal range of 0-50 in (a) was visualized in (c). In addition to the area whose signal intensity was 50 in (a), the area whose signal intensity was between 51 and 255 in (a) was also represented in white in (c). (f) Brightness-enhanced image of (e). The brightness-enhanced image was prepared in a similar manner to (c). (g) The images in (c) and (f) were superimposed with green and red pseudo-colors, respectively.

Figure 2. Spatiotemporal visualization of FAO activity in the liver

FAO activities of the liver in the (A–C) Ctrl, (D–F) Pema, (G–I) Fasting_24h, (J–L) Fasting_72h, and (M-O) Eto groups were visualized at 0, 2, and 7 min ($\lambda_{ex}/\lambda_{em}$ = 820/415-485 nm). See Supplemental Video S2. Multiphoton microscopy observation began at 0 min. FAOBlue was injected at 0.5 min. Representative microscopic images are shown. White dashed circles in (A), (D), (G), (J) and (M) indicate pericentral regions (Scale bars: 100 µm). FAO: fatty acid β-oxidation, Ctrl: Control, Pema: Pemafibrate, Fasting_24h: fasting for 24 hours, Fasting_72h: fasting for 72 hours, Eto: Etomoxir.

Figure 3. Spatiotemporal quantification of FAO activity in the liver and real-time PCR analyses of FAO-related genes

(A–D) FAO activities of the liver in the Ctrl, Pema, Fasting_24h, Fasting_72h, and Eto groups shown in Figure 2 and Supplemental Video S2 were spatiotemporally quantified. (A) Time courses of the fluorescence intensity of hepatocytes in the periportal and pericentral regions. Black arrows indicate the time point when FAOBlue was injected. (B) AUCs of (A) are shown. (C) Maximum increasing slope of (A) in each animal. (D) Time of first detection of FAO-derived fluorescence in each animal. (E) Real-time PCR analyses of FAO-related genes in the liver. All results are presented as a scatter plot with means ± SDs (N = 5-8 biological replicates in each group: * $P < 0.05$, ** $P < 0.01$, Dunnett's test). n/a: not available, ns: not significant, Ref: reference, AUC: area under the curve.

Figure 4. Spatiotemporal visualization of liver fluorescence after injection of 7-HC through the right jugular vein

Mice were pretreated as in the FAOBlue administration experiments and then injected with 7-HC through the right jugular vein. (A–C) Ctrl, (D–F) Pema, (G–I) Fasting_24h, (J–L) Fasting_72h, and (M-O) Eto groups. Representative microscopic images at 0,1, and 7 minutes are shown, with 7-HC being injected at 0.5 minutes ($\lambda_{ex}/\lambda_{em}$ = 820/415-485 nm). White dashed circles indicate pericentral regions (Scale bars: 100 µm). See Supplemental Video S3.

Figure 5. Spatiotemporal quantification of liver fluorescence after injection of 7-HC through the right jugular vein

569   (A–D) Fluorescent intensity of the liver in the Ctrl, Pema, Fasting_24h, Fasting_72h, and Eto

570   groups shown in Figure 4 and Supplemental Video S3 were spatiotemporally quantified. (A)

571   Time courses of the fluorescence intensity of hepatocytes in the periportal and pericentral

572   regions. Black arrows indicate the time point when 7-HC was injected. (B) AUCs of (A) are

573   shown. (C) The time to peak fluorescence and (D) the rate of decay from the fluorescence peak

574   are presented (N = 3 biological replicates in each group: ns, not significant: Dunnett's test).

575

Figure 1

Figure 2

	0 min	2 min	7 min
Ctrl	A	B	C
Pema	D	E	F
Fasting_24h	G	H	I
Fasting_72h	J	K	L
Eto	M	N	O

0   Grayscale   255

Figure 3

Figure 4

	0 min	1 min	7 min
Ctrl	A	B	C
Pema	D	E	F
Fasting_24h	G	H	I
Fasting_72h	J	K	L
Eto	M	N	O

0 Grayscale 255

Figure 5

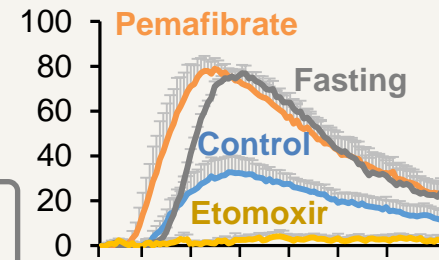# Spatiotemporally quantitative *in vivo* imaging of mitochondrial fatty acid β-oxidation at cellular-level resolution in mice